

# Cosmic ray flux anisotropies caused by astrospheres

K. Scherer<sup>a,\*</sup>, R.D. Strauss<sup>b</sup>, S.E.S. Ferreira<sup>b</sup>, H. Fichtner<sup>a</sup>

<sup>a</sup>*Institut für Theoretische Physik IV, Ruhr-Universität Bochum, Germany.*

<sup>b</sup>*Centre for Space Research, North-West University, Potchefstroom, South Africa*

---

## Abstract

Huge astrospheres or stellar wind bubbles influence the propagation of cosmic rays at energies up to the TeV range and can act as small-scale sinks decreasing the cosmic ray flux. We model such a sink (in 2D) by a sphere of radius 10 pc embedded within a sphere of a radius of 1 kpc. The cosmic ray flux is calculated by means of backward stochastic differential equations from an observer, which is located at  $r_0$ , to the outer boundary. It turns out that such small-scale sinks can influence the cosmic ray flux at the observer's location by a few permille (i.e a few 0.1%), which is in the range of the observations by IceCube, Milagro and other large area telescopes.

*Keywords:* Cosmic ray anisotropy, astrospheres, Cosmic ray transport

---

## 1. Introduction

Large area cosmic ray detectors like the Tibet Air shower experiment, IceCube/IceTop, Milagro and HAWC, among others observe a multipole like anisotropy of the high energy cosmic ray flux (CRF) over the entire sky (Iuppa and ARGO-YBJ Collaboration, 2013; Abeysekara et al., 2014; Ben-Zvi, 2014; Desiati, 2014; Di Sciascio and Iuppa, 2014; Di Sciascio, 2015; López-Barquero et al., 2015; IceCube Collaboration et al., 2016). The energies of interest are in the TeV range which vary on small-scales by a few permille (‰) for details see Toscano and IceCube Collaboration (2012) and Iuppa et al. (2012).

At higher energies (PeV) anisotropies were also found (Giacinti and Sigl, 2012; Zotov and Kulikov, 2012; Aartsen et al., 2013; Glushkov and Pravdin, 2013) which may be still of Galactic origin. Even at energies around EeV, anisotropies in the arrival directions are observed (e.g. Pierre Auger Collaboration et al., 2011, 2013), which may be at the transition to an extragalactic origin of the cosmic rays. These high energies are not taken under consideration here.

A few explanations have been proposed, either related to interstellar magnetic field variations (Amenomori et al., 2011), intermediate turbulence (Biermann et al., 2015) due to the heliotail (Desiati and Lazarian, 2014; Zhang et al., 2014; Pogorelov et al., 2015; Schwadron et al., 2015). A detailed analysis of the power spectrum is discussed in Ahlers and Mertsch (2015) where the authors showed that the strength of the power spectrum is related to the diffusion tensor. Harari et al. (2016) discussed turbulent magnetic fields as the cause of small angular scale variations, while Battaner et al. (2015) correlated the anisotropy to the global cosmic ray flux.

There are small-scale variations (tens of degrees) and even tiny-scale variations about a degree or less in the interstellar medium caused by astrospheres, planetary nebulae and similar inhomogeneities (Stanimirović et al., 2010; Haverkorn and Spangler, 2013; Linsky and Redfield, 2014). In the following we explain how such variations – due to the presence of astrospheres – act as small-scale sinks (S3) of CRF in the interstellar medium, can lead to such anisotropies.

Huge astrospheres or stellar wind bubbles have been discussed for example in Mackey et al. (2015)

---

\*Corresponding author

and Scherer et al. (2016), especially their influence to the CRF was studied in Scherer et al. (2015) for the case of  $\lambda$  Cephei. The latter authors found that the CRF at energies up to 100 TeV is affected on scales below 1 pc along the stagnation line of the astrosphere. Because the discussed astrosphere of  $\lambda$  Cephei is special, in the sense that the relative motion between the star and the ISM is high (about 80 km/s), and the bow shock distance is about 1 pc. Most of the astrospheres of hot stars do not show any relative motion and build stellar wind bubbles of the order of 10-100 pc. These bubbles have very high compression ratios (Toalá and Arthur, 2011) and thus can effectively act as sinks for the CRF. The CRF is already affected directly beyond the bowshock, see Scherer et al. (2011), Strauss et al. (2013), and Luo et al. (2015), and thus the effective modulation in astrospheres starts directly behind the bow shock, and not as in the heliosphere at the heliopause (Kóta and Jokipii, 2014; Potgieter, 2014).

Here we setup a model where we study the transport of cosmic rays (CRs), when there is a S3 between the outer boundary and the observer. In section 2 we present the model in detail, while in section 3 the numerical scheme is discussed. In section 4 we study the results for a range of appropriate parameters (given in Table 1 below) and finally we give a résumé in section 5

## 2. The model

The basic scenario of our model is shown in Fig. 1: CRs, propagate from their sources (specified at  $r_{\text{boundary}} = r_b$ ) towards Earth, assumed to be at the origin. We now place a spherical inhomogeneity (S3, most likely, an astrosphere), with a radius of  $r_{\text{astrosphere}} = r_a$ , at a distance of  $d_{\text{astrosphere}} = d_a$  from the Sun. The position of the astrosphere is also specified by the angle  $\varphi_{\text{astrosphere}} = \varphi_a$ , measured from the  $y$ -axis. We do not calculate the intensity at Earth itself (this would be a point in this set-up), but at an *observer's* position, specified by  $r_{\text{observer}} = r_o$  and the angle  $\varphi_{\text{observer}} = \varphi_o$ . It is assumed that any anisotropies at  $r_o$  will be *frozen-in* and be directly observable at Earth; a good approximation if the

particle mean free path is  $\lambda > r_o$ , which is usually larger in the ISM Scherer et al. (for the local influence of different mean free pathes on astrosphere, see 2015). We assume that the S3 influence the particle intensity, i.e. some particles that interact with the S3 will be lost. This could be due to e.g. adiabatic energy losses suffered in the astrosphere's expanding stellar wind or due to catastrophic losses in a denser medium close the host star. Independent of the process, we assume that the intensity of CRs, when interacting with the astrosphere, will decrease.

The diffusion coefficient in the transport equation depend, in general, on the magnetic field structure inside an astrosphere, which is not known. Because we are not interested in the details of the CRF inside the astrosphere, we simulate the CRF through it by an extinction coefficient. For details see below.

As already mentioned, we require  $\lambda > r_o$  for our simulation. Furthermore also assuming  $\lambda < r_b$ , we can safely consider that the resulting anisotropies will be small and use a Parker-like transport equation (Parker, 1965) to describe their transport in the turbulent interstellar medium (we therefore have the scaling  $r_o < \lambda < r_b$ ). For a nearly isotropic CR distribution function  $f$ , we solve

$$\frac{\partial f}{\partial t} = \nabla \cdot (\mathcal{K} \cdot \nabla f) - \mathcal{Q}f \quad (1)$$

which includes the loss-rate  $\mathcal{Q}$  due to CRs interacting with the S3. Assuming a 2D Cartesian geometry and a mean magnetic field  $\vec{B} = B\hat{y}$ , the diffusion tensor reduces to

$$\mathcal{K} = \begin{bmatrix} \kappa_{\perp} & 0 \\ 0 & \kappa_{\parallel} \end{bmatrix} \quad (2)$$

For simplicity, we assume  $\kappa_{\parallel} (= \kappa_y)$  and  $\kappa_{\perp} (= \kappa_x)$  to be constant and to be linearly related via  $\kappa_{\perp} = \eta\kappa_{\parallel}$ .

## 3. The numerical solver

We solve Eq. 1 by means of stochastic differential equations (SDEs). The set of SDEs, being equivalent to Eq. 1, is, for  $q \in \{x, y\}$ , simply

$$dq = dW_q \sqrt{2\kappa_q} \quad (3)$$

where  $dW_q \approx \mathcal{R}_q \sqrt{\Delta s}$  are Wiener processes and  $\mathcal{R}_q$  independent, normally distributed, random numbers. For details of this numerical approach (see e.g. Strauss et al., 2011a; Kopp et al., 2012). We solve these equations backwards time, where backwards in time is labeled by  $s$ .

In general, a loss term is handled in the SDE formulation by keeping track of the so-called *particle amplitude*,  $\alpha_i$ , for each pseudo particle (labeled by  $i$ ) during the integration process. I.e., starting initially at  $\alpha_i(s=0) = 1$ , this quantity is updated as

$$\alpha_i(s + \Delta s) = \alpha_i(s) \exp(-\mathcal{Q}\Delta s) \quad (4)$$

We do, however, not yet know the precise form of the loss-rate, neither the amount of time CRs will spend in such inhomogeneities ( $\Delta s$ , which will depend on the transport conditions in the inhomogeneities themselves) so we approximate Eq. 4 as

$$\alpha_i(s + \Delta s) \approx \alpha_i(s) (1 - \chi) : x, y \in \text{S3}. \quad (5)$$

where we have defined an extinction coefficient  $\chi$  ( $0 \leq \chi \leq 1$ ), that is the fraction of the CR particles lost when a S3 was encountered, i.e.  $\chi = 1$ , or equivalently  $\chi = 100\%$ , means that all particles that encountered the S3 were lost.

The numerical time step in the SDE scheme,  $\Delta s$ , determines what scale of structures will be sampled by these pseudo-particles in configuration space. In order to sample the relevant spatial features in our model set-up (i.e. pseudo-particles should not *jump* across the S3, but sample it continuously), we follow Strauss et al. (2013) and implement a variable time step as

$$\Delta s = \sigma \frac{\mathcal{L}^2}{\max\{\kappa_{\parallel}, \kappa_{\perp}\}} \quad (6)$$

where  $\mathcal{L}$  is the spatial extend of the smallest structure in the model and  $\sigma$  a constant, usually chosen to be  $\sigma = 0.5$  or smaller.

The solution of the transport equation at any point in space is now calculated, in the steady-state limit, as

$$f(x, y) \approx \frac{1}{N} \sum_{i=1}^N \alpha_i f_{\text{boundary}} \quad (7)$$

where  $N$  is the number of pseudo-particles (a term for each numerical realisation of the set of SDEs, not a physical CR particle) solved and  $f_{\text{boundary}}$  is the boundary value, specified at  $r_b$ . We simply use  $f_{\text{boundary}} = 1$  without any loss of generality.

We can easily estimate the statistical error related to this method of solution by assuming Poisson statistics for the resulting distribution (a fair approximation when looking at the results of e.g. Strauss et al. (2011b)),  $N = N \pm \sqrt{N}$ , so that Eq. 7 is modified to become

$$f(x, y) \approx \frac{1}{N} \sum_{i=1}^N \alpha_i \left( 1 \pm \frac{1}{\sqrt{N}} \right), \quad (8)$$

and the resulting *error bar* plotted with the intensities in the next sections. To get our results accurate to the permille range, we therefore need, at least,  $N = 10^6$ , pseudo-particles so, for the simulation in this work, we use  $N = 10^7$  such particles at each phase-space position where the intensity is calculated.

## 4. Results

Because we study a large set of parameters such as the variation of the distance  $d_a$  to the astrosphere, its size  $r_a$ , the angle to the observe  $\varphi_a$  as well the ratio  $\eta$  of the perpendicular to the parallel diffusion coefficient, and finally the loss rate  $\chi$  inside the astrosphere, we start with a reference solution (RS) with  $d_a = 600$  pc,  $r_a = 10$  pc,  $\varphi_a = 45^\circ$ ,  $\eta = 0.5$ , and  $\chi = 100\%$ . Other model parameters relative to the RS is shown in Table 1.

The variation of the CRF of the RS is shown in Fig. 2 together with the numerical error bars (see Eq. 7). The error bars are similar in all subsequent models and not shown further. In Fig. 3 to 4 the RS is, as reference, always shown as the black line.

The RS shown in Fig. 2 is the solution of the SDE equation, as a function of  $\varphi_o$ , at  $r_o = 10$  pc. The solution is normalised to its average value (averaged over  $\varphi_o$ ), that is,  $j/\langle j \rangle > 1$  shows an excess of particles *with respect to the average of  $j$  over all  $\varphi_o$ 's*. Note that, in the current model, the differential intensity  $j$ , is directly proportional

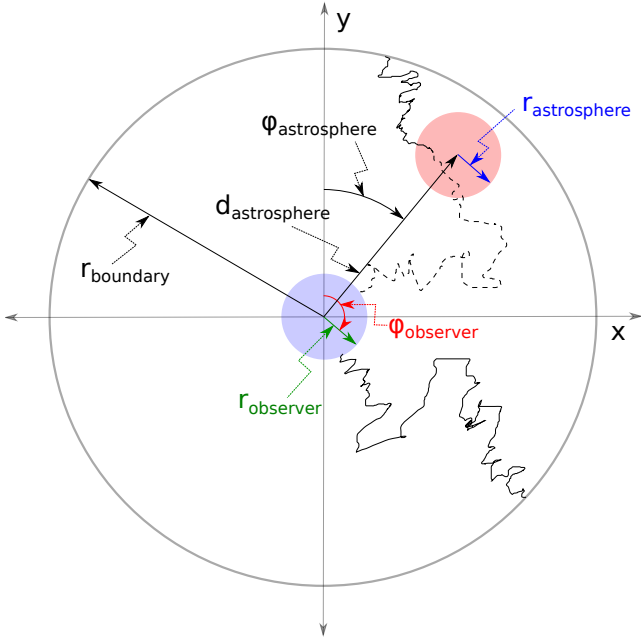


Figure 1: The model setup. The astrosphere (or S3) is located at a distance  $d_a$  from the observer and has a radius of  $r_a$ . The whole integration area is a sphere with radius  $r_b$ . The magnetic field is directed along the  $y$ -axis and the astrospheres is offset from the  $y$ -axis by an angle  $\varphi_a$ . The inner boundary is at  $r_o$ , which is much smaller than the CR mean free path. The two scatter lines show the path of a pseudo particles: one travels unhindered from  $r_b$  to  $r_o$ , while the other interacts with the astrosphere and does no longer contribute (fully) to the CRF at  $r_o$ . The dotted line shows a possible path of that pseudo-particle.

to the distribution function  $f$ . The black lines horizontal show the permille range.

The solutions depend on the ratios  $\eta = \kappa_{\perp}/\kappa_{\parallel}$  and  $\eta/\chi$ . This is because, for a diffusion equation, with constant (time independent) coefficients and boundary conditions, the steady state solution is only determined by the boundary conditions. When, in future, we generalize Eq. 1 to include energy losses in the interstellar medium, and implement more realistic parametrisations of the energy losses in S3, the magnitude of  $\kappa_{\parallel}, \kappa_{\perp}$  may play an important role (here the ratio  $\kappa/Q$  plays that role).

The RS show some interesting features: The variation is in the permille range as required by the observations. The most exciting fact is, that the S3, with a filling factor  $F = r_a^2/r_b^2 \approx 3 \cdot 10^{-4}$  (defined as the ratio of the area of the S3 to that of the large sphere, see section 4.1 below), influences the variation along the observer angle af-

#	$r_a$ pc	$d_a$ pc	$\varphi_a$ °	$\eta$	$\chi$ %	A ‰	$\beta$ °
0	10	600	45	0.5	100	-2.6	- 70
1	10	400	45	0.5	100	-5.2	- 65
2	10	800	45	0.5	100	-1.1	- 70
3	10	600	0	0.5	100	-2.6	- 0
4	10	600	90	0.5	100	-2.3	- 90
5	10	600	135	0.5	100	-2.6	- 110
6	10	600	180	0.5	100	-2.7	- 180
7	5	600	45	0.5	100	-2.2	- 70
8	25	600	45	0.5	100	-3.8	- 70
9	50	600	45	0.5	100	-0.5	- 70
10	10	600	45	0.02	100	-0.4	- 90
11	10	600	45	1.0	100	-2.4	- 45
12	10	600	45	0.5	0	0	-
13	10	600	45	0.5	25	-0.6	- 70
14	10	600	45	0.5	50	-1.2	- 70
15	10	600	45	0.5	75	-1.8	- 70
16	10	600	45/135	0.5	100	-5.1	- 90
17	10	600	45/225	0.5	100	0	-

Table 1: The parameters used for the different models. Model 0 is the RS and each vertical line separates a new set of parameters: models 1 and 2 vary the distance, models 3 to 6 the position angle, i.e. the magnetic field direction with respect to the S3, model 7 to 9 the size of the S3, model 10 and 11 the the ratio  $\eta$  between the perpendicular to parallel diffusion, and models 12 to 15 the extinction coefficient  $\chi$ . The last two columns are the parameters of a fit to  $-A \cos(\varphi - \beta)$  (see section 4.1 below). In models 16 and 17 two astrospheres are modeled simultaneously, which are identically to model 0, except is position angle.

fects over the entire range, with a maximum at  $\approx 250^\circ$ , which is the undisturbed CRF flux, and a minimum at  $\varphi_{\min} \approx 70^\circ$ . The latter has an offset  $\Delta\varphi = \varphi_{\min} - \varphi_o$  of about  $25^\circ$  to the direction of the S3. This is caused by the orientation of the magnetic field along the  $y$ -axis and the fact, that the cosmic rays are not only diffusing along the magnetic field but also perpendicular to it. In our setup of the model (Fig. 1) two possible paths of a pseudo-particle are indicated: one which is not affected by the S3 (solid line) and another one which is (solid and then dashed line). The pseudo-particle would follow the dashed line if it is not absorbed in the S3. This is the case when we change the extinction coefficient  $\chi$  for some

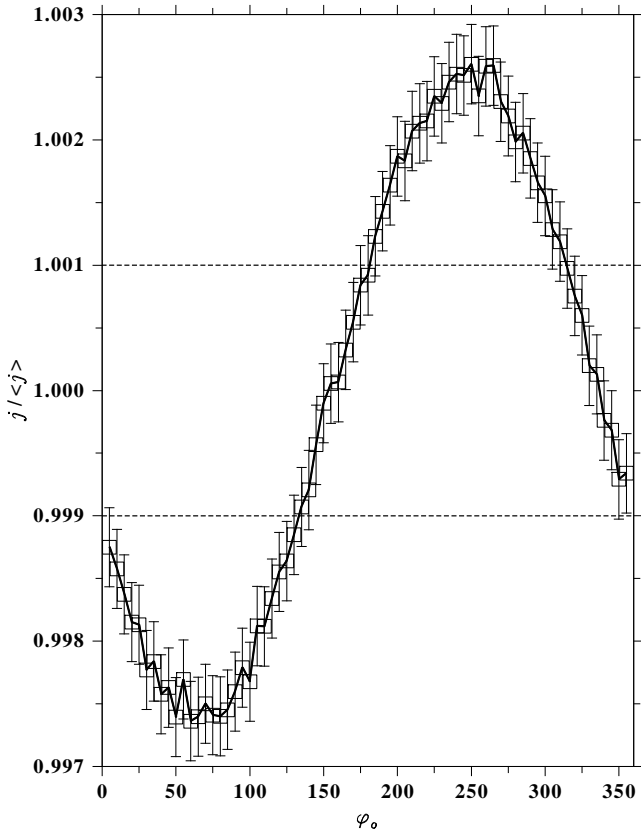


Figure 2: Reference solution for the CRF. To guide the eye the red lines show the 0.1% level. As reference values we take a distance to the S3 of 600 pc, a radius of 10 pc, an angle from the y-axis of  $\varphi = 45^\circ$ , a ratio of  $\eta = \kappa_\perp / \kappa_\parallel = 0.5$ , and the loss of the CRF flux inside the S3  $\chi = 100\%$ . The variation of the CRF is about  $\pm 0.3\%$  along the observer angle  $\varphi$ . Because the magnetic field is directed along the y-axis, the minimum is shifted by about 25% from the actual position, in terms of  $\varphi_o$  of S3.

particles.

Another exciting feature is the extent of the minimum (maximum) of the CRF flux, it can be as broad as some ten degrees. This is also compatible within the range of the observed angular size of the CRF (see, e.g. IceCube Collaboration et al., 2016).

To study these effects further we varied first the distance of the S3 to  $d_a = 400$  pc, which can be seen in the left panel of Fig. 1 (model 1, red line) and to  $d_a = 800$  pc (model 2, blue line). The amplitude of the curves increases (decrease) with decreasing (increasing) distance compared to the RS, but their minima and maxima remain more or less at the same position. The increase in the amplitude is not linear: it is about a factor 2 larger

for model 2 and about a factor 0.4 smaller for model 1 compared to RS. The reason is that a closer S3 blocks relatively more CR because of its apparent large area with respect to the observer. These effects are expected: the further away a S3 is, the smaller is the CRF variation.

In the middle panel we show the variation in the position angle  $\varphi_a$ . This changes the orientation of the magnetic field relative to S3, and thus the transport of CR along the magnetic field is reduced as can be seen by the magenta line, where the propagation from the S3 to the observer is perpendicular to the magnetic field and thus the amplitude of the CRF is slightly reduced. The parallel and anti-parallel propagation effects shown by the red and cyan lines seem to be marginally higher than the RS, but that is inside the error bars. Nevertheless, the minima (maxima) of the models with non-parallel propagation (black and blue lines) deviate from the location of the position angle by  $\Delta\varphi \approx 25^\circ$  for  $\varphi_a = 45^\circ$  and  $\Delta\varphi \approx -25^\circ$  for  $\varphi_a = 135^\circ$ , while the model the perpendicular propagation has its minimum at  $\Delta\varphi \approx 0^\circ$ . Thus a varying magnetic field orientation influences the position of the CRF-minima (maxima) from  $0^\circ$  up to  $\approx 25^\circ$ . Thus determining the position of the sinks by observations requires a good knowledge of the interstellar magnetic field.

Finally, we varied the ratio  $\eta$  of the perpendicular to parallel diffusion coefficient and the extinction coefficient  $\chi$  shown in Fig. 4. The variation of  $\eta$  is shown in the left panel and that of  $\chi$  in the middle panel. It can be seen that for very small ratios  $\chi$  the amplitude of the CRF is below 0.1% (red line, right panel) and that the minima (maxima) are shifted to much larger offsets than changing the position angle. If both diffusion coefficient are equal ( $\kappa_\parallel = \kappa_\perp$ ) the extrema of the CRF are a little smaller than that of the RS and are not offset from the position angle  $\Delta\varphi \approx 0^\circ$ . The latter is due to the fact, that if  $\eta = 1$  both diffusion coefficients are equal and thus there is no preferred direction for diffusion (isotropic or scalar diffusion).

In the middle panel of Fig. 4 the extinction coefficient is changed. This varies only the amplitude from zero for no extinction ( $\chi = 0\%$ ) to

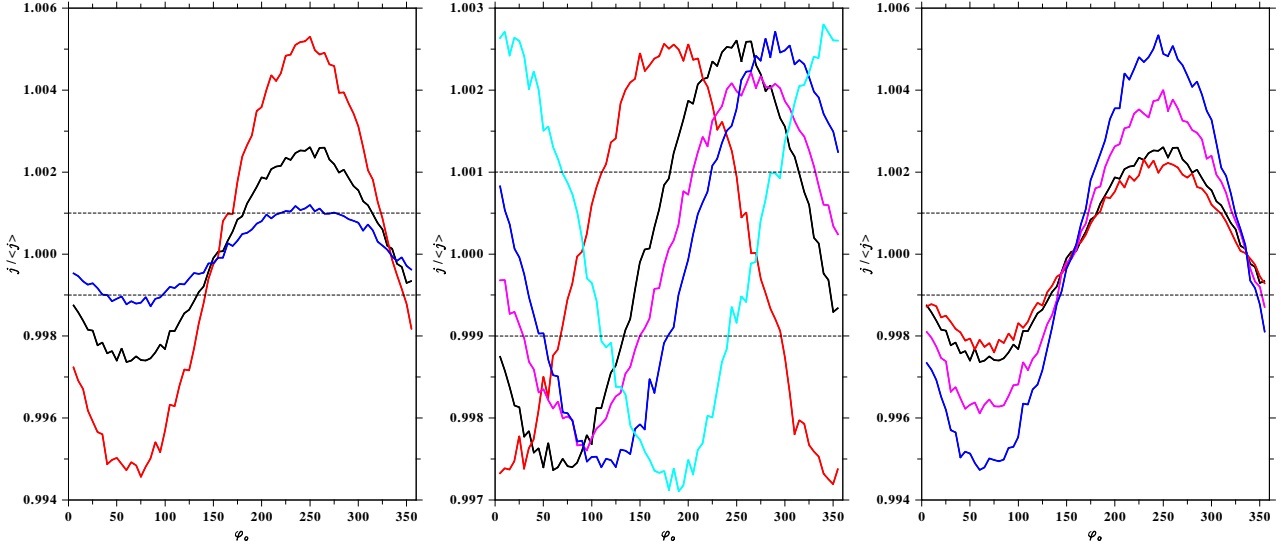


Figure 3: Variation of astrosphere distance (left panel), the angle with respect to the magnetic field  $\varphi_a$  (middle panel), and the size of S3  $r_a$  (right panel). The colour coding in the left panel is:  $d_a = 400$  pc red line and  $800$  pc blue line. The colours in the middle panel vary for  $\varphi_a = 0, 45, 90, 135, 180$  degree as red, black, magenta, blue, and cyan, respectively. Finally those in the right panel, where the size varies for  $r_a = 5, 10, 25, 50$  pc, as red, black, magenta, and blue. The black lines always indicate the RS. The scales on the  $y$ -axis differ.

that of our RS. An extinction coefficient of  $\chi = 0$  or  $\chi = 25\%$  are below the  $0.1\%$  level, while that of  $\chi = 50\%, 75\%$  and  $\chi = 100\%$  lead to variations of the CRF flux in the observed range (for a discussion see below section 4.1).

We just shortly present the case (model 16) if we have two S3 locate at  $\varphi_{a,1} = 45^\circ$  and  $\varphi_{a,2} = 225^\circ$  (see Fig: 4, right panel). Because the diffusion depends on the direction and not on the orientation of the magnetic field, it is identical for both S3 and thus where the CRF of one S3 shows a maximum, the other S3 has a minimum, and analogously  $\varphi_o$  both variations add to zero. Thus the result is like that of a “destructive” interference. The absolute CRF should be lower compared to a single S3, but the absolute flux cannot be studied with the present setup of our model. Another case, where the astrospheres are located at  $\varphi_{a,1} = 45^\circ$  and  $\varphi_{a,2} = 135^\circ$  (see Fig: 4, right panel) gives an “constructive” interference and an additional phaseshift compared to the RS. We presented these two cases here to show the capability of our model, but do not discuss it further in the present context. Nevertheless, the above examples show, that we can get a kind of interference of different sinks, which can be decom-

posed into a multipole power spectrum (Ahlers and Mertsch, 2015).

#### 4.1. Summary of the parameter study

We fitted the function  $-A_i \cos(\varphi - \beta_i)$  to each CRF in Figs. 2 to 4 (not shown), where  $i$  indicates the model number. With the help of that function, it is easier to discuss the amplitude  $A_i$  and phase shift  $\alpha_i$ . The values of  $A_i$  and  $\alpha_i$  are given in the last two rows of Table 1.

We can identify two geometrical effects: the distance to the S3 and its radius: The amplitudes  $A_i$  of the normalised CRF varies with both the distance and the size of the S3 (models 1 and 2, see left panel and models 7 to 9 right panel of Fig. 3). The variations in the CRF amplitude are as expected: larger (smaller) for smaller (larger) distances or sizes. Our expectation is that the amplitudes depend on the opening angle of the S3 as seen from the observer. But because of the few examples it is not possible to study these effect empirically.

The physics of the transport of CRs are influenced by the extinction parameter  $\chi$ , which already gives amplitudes in the permille range, when it is larger than  $25\%$ , as can be expected for S3’s (models 12–14, middle panel of Fig. 4).

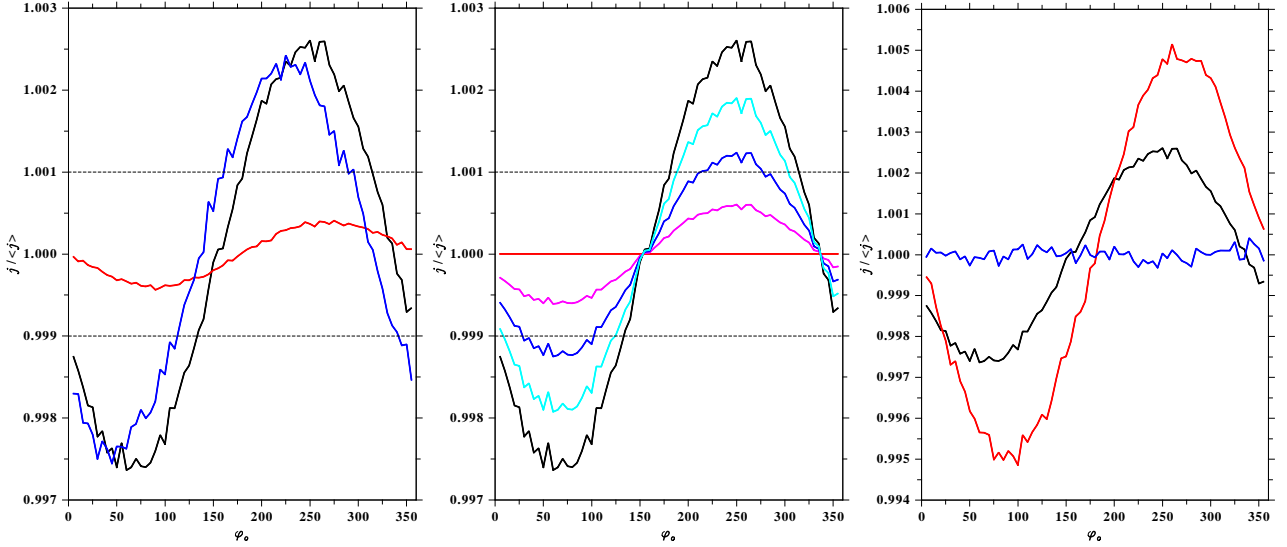


Figure 4: Variation of the ratio  $\eta$  of perpendicular to parallel diffusion coefficients (left panel), the extinction coefficient  $\chi$  (middle panel) and the effect of two S3 (right panel). The colours for  $\eta = 0.02, 0.5, 1$  are red, black, blue (left panel), that of  $\chi = 0, 25, 50, 75, 100$ , red, magenta, blue, cyan, black. Again the black line represents the RS. In the right panel we have modeled two astrospheres separated by  $90^\circ$  and  $180^\circ$ . The latter normalised flux does not show any variation, because of the “destructive” interference, while the former has an “constructive” interference and an additional shift of the maxima/minima.

This effect is also as expected, the larger the extinction coefficient the larger is the amplitude.

The ratio of the perpendicular to parallel diffusion coefficient is a parameter, which is important not only for the amplitude but also for the offset  $\Delta\varphi$  (models 10 and 11, right panel of Fig. 4). This can be understood as an effect of the parallel/perpendicular diffusion, and, thus, how easy CRs can travel along the respective direction, influencing the amplitude and the offset. Thus, it again turns out that the perpendicular diffusion coefficient plays an important role when modeling the galactic cosmic ray transport, as already discussed in e.g. Effenberger et al. (2012), Kumar and Eichler (2014), and Mertsch and Funk (2015).

Finally, the orientation of the magnetic field plays an important role affecting the offset  $\Delta\varphi$ . This is simulated by the position of the S3 relative to the x-axis (model 3 to 6 middle panel of Fig. 3). This can be explained by the fact that there is a more efficient diffusion in the parallel direction, as long as  $\eta \neq 1$ , which then causes the offset.

All the models discussed here show a relatively flat minimum (maximum) with an extension of a few degrees, where the normalised CRF variation

are inside the error bars (only shown in Fig. 2 for the RS). Thus, from an observational point of view the sources can have a large angular extent.

Thus we have five parameters ( $d_a, r_a, \varphi_a, \eta$ , and  $\chi$ ) which influence the amplitude and offset of the CRF. We have varied them individually with respect to the RS, but did not study simultaneous variations of these parameters. This can be done when observational data are available. Here we demonstrated the effects to the CRF of a S3 with a small filling factor of  $F = 10^{-4}$ , and conclude that such a S3 is a possible explanation for the observed small-scale variations.

Replacing the sinks by appropriate sources we anticipate to get inverse results, because at the source position we expect to have the largest flux going to a minimum opposite to it. The phase shift should also be equal to that of the sinks discussed here. We will study it in a forthcoming paper.

We studied additionally, the CRF when two S3 are present (model 16 and 17, right panel of Fig. 4) which show something like an interference. A detailed study of two or more S3 would go far beyond the scope of this work, but the two ex-

amples indicate that a Fourier decomposition of the signal along the observer angle can give some hints of the involved sinks.

In Eq. 1 we used a constant parallel diffusion coefficient  $\kappa_{\parallel}$  and loss term  $\mathcal{Q}$ , and, thus get an “energy dependence” by increasing (decreasing)  $\kappa_{\parallel}$  relative to  $\mathcal{Q}$ , because of the quasi-stationarity of Eq. 1. For more realistic scenarios one can include an energy dependent diffusion, but for the higher energies this does not play an essential role.

The filling factor  $F$  is different when we go from a 2D scenario to a 3D one. Then one needs a sphere with a radius of approximately 50 pc to get the same filling factor. Also the diffusion perpendicular to the galactic plane can influence our estimates. Assuming that cosmic rays diffusing perpendicular to the galactic disk escape before they can be detected and the CRF is confined in the galactic disk, then the modulation is approximately 2D and we expect an similar result.

In the above models we used, except for models 12 to 15 a extinction rate of 100%, which may be too large and one would expect it to be in range 25% to 50%. But this is only a sophisticated guess, because as far as we know there is no model in which an astrosphere or other object blocks (partially) the CRF. Only Scherer et al. (2015) have calculated the CRF along the stagnation line into the astrosphere around  $\lambda$  Cephei up to an inner boundary of 0.03 pc. Thus, to get a better estimate on the extinction factor of the CRF, we need to extend our calculations of the modulation to a point outside of the astrosphere.

## 5. Resume

We simulated the cosmic ray flux in a 1 kpc sphere, when small-scale sinks are located inside this sphere. We showed that there is a depletion of the CRF in the order of a few permille. Moreover, it turned out that such a small obstacle, for example, an astrosphere with a radius of 10 pc influences the entire observer angle, and is not only a spike, but a sinusoidal variation. The flat minimum of these variations have an extension of a few degree.

Thus, obstacles with filling factors of  $F \approx 10^{-4}$  lead to the observed variations in the permille range, except when the ratio of the diffusion coefficients ( $\eta < 0.02$ ) or the extinction coefficient ( $\chi < 25\%$ ) is too small. But then an increase in the size or distance to the S3 can compensate the low CRF variation.

We have demonstrated, that small-scale sinks in the ISM can lead to the observed multipole character of the CRF. Unfortunately, due to the fact that the arrival direction of the CRF in the minimum does not necessarily coincide to with the location of the obstacle, the identification of the latter is complicated.

We have shown that in the above simplified scenario, we obtain quite promising results in describing the CRF anisotropy. Thus, we will continue the study in future implementing more realistic scenarios.

## Acknowledgement

KS is grateful to the *Deutsche Forschungsgemeinschaft, DFG* for funding the projects SCHE 334/9-1 and SCHE334/9-2. This work is based on research supported in part by the National Research Foundation (NRF) of South Africa. This work was carried out within the framework of the bilateral BMBF-NRF project “Astrohel” (01DG 15009) funded by the Bundesministerium für Bildung und Forschung. The responsibility of the content of this work is with the authors.

## References

- Aartsen, M. G., Abbasi, R., Abdou, Y., Ackermann, M., Adams, J., Aguilar, J. A., Ahlers, M., Altmann, D., Andeen, K., Auffenberg, J., et al., Mar. 2013. Observation of Cosmic-Ray Anisotropy with the IceTop Air Shower Array. *Astrophys. J.* 765, 55.
- Abeysekara, A. U., Alfaro, R., Alvarez, C., Álvarez, J. D., Arceo, R., Arteaga-Velázquez, J. C., Ayala Solares, H. A., Barber, A. S., Baughman, B. M., Bautista-Elivar, N., Belmont, E., BenZvi, S. Y., Berley, D., Bonilla Rosales, M., Braun, J., Caballero-Mora, K. S., Carramiñana, A., Castillo, M., Cotti, U., Cotzomi, J., de la Fuente, E., De León, C., DeYoung, T., Diaz Hernandez, R., Díaz-Vélez, J. C., Dingus, B. L., DuVernois, M. A., Ellsworth, R. W., Fiorino, D. W., Fraija,

- N., Galindo, A., Garfias, F., González, M. M., Goodman, J. A., Gussert, M., Hampel-Arias, Z., Harding, J. P., Hüntemeyer, P., Hui, C. M., Imran, A., Iriarte, A., Karn, P., Kieda, D., Kunde, G. J., Lara, A., Lauer, R. J., Lee, W. H., Lennarz, D., León Vargas, H., Linnemann, J. T., Longo, M., Luna-García, R., Malone, K., Marinelli, A., Marinelli, S. S., Martinez, H., Martinez, O., Martínez-Castro, J., Matthews, J. A. J., McEnery, J., Mendoza Torres, E., Miranda-Romagnoli, P., Moreno, E., Mostafá, M., Nellen, L., Newbold, M., Noriega-Papaqui, R., Ocegüera-Becerra, T., Patricelli, B., Pelayo, R., Pérez-Pérez, E. G., Pretz, J., Rivière, C., Rosa-González, D., Ruiz-Velasco, E., Ryan, J., Salazar, H., Salesa Greus, F., Sandoval, A., Schneider, M., Sinišić, G., Smith, A. J., Sparks Woodle, K., Springer, R. W., Taboada, I., Toale, P. A., Tollefson, K., Torres, I., Ukwatta, T. N., Villaseñor, L., Weisgarber, T., Westerhoff, S., Wisher, I. G., Wood, J., Yodh, G. B., Younk, P. W., Zaborov, D., Zepeda, A., Zhou, H., HAWC Collaboration, Dec. 2014. Observation of Small-scale Anisotropy in the Arrival Direction Distribution of TeV Cosmic Rays with HAWC. *Astrophys. J.* 796, 108.
- Ahlers, M., Mertsch, P., Dec. 2015. Small-scale Anisotropies of Cosmic Rays from Relative Diffusion. *Astrophys. J. Lett.* 815, L2.
- Amenomori, M., Bi, X. J., Chen, D., Cui, S. W., Danzengluobu, Ding, L. K., Ding, X. H., Fan, C., Feng, C. F., Feng, Z., Feng, Z. Y., Gao, X. Y., Geng, Q. X., Gou, Q. B., Guo, H. W., He, H. H., He, M., Hibino, K., Hotta, N., Hu, H., Hu, H. B., Huang, J., Huang, Q., Jia, H. Y., Jiang, L., Kajino, F., Kasahara, K., Katayose, Y., Kato, C., Kawata, K., Labaciren, Le, G. M., Li, A. F., Li, H. C., Li, J. Y., Liu, C., Lou, Y., Lu, H., Meng, X. R., Mizutani, K., Mu, J., Munakata, K., Nanjo, H., Nishizawa, M., Ohnishi, M., Ohta, I., Ozawa, S., Saito, T., Saito, T. Y., Sakata, M., Sako, T. K., Shibata, M., Shiomi, A., Shirai, T., Sugimoto, H., Takita, M., Tan, Y. H., Tateyama, N., Torii, S., Tsuchiya, H., Udo, S., Wang, B., Wang, H., Wang, Y., Wang, Y. G., Wu, H. R., Xue, L., Yamamoto, Y., Yan, C. T., Yang, X. C., Yasue, S., Ye, Z. H., Yu, G. C., Yuan, A. F., Yuda, T., Zhang, H. M., Zhang, J. L., Zhang, N. J., Zhang, X. Y., Zhang, Y., Zhang, Y., Zhang, Y., Zhaxisangzhu, Zhou, X. X., Jan. 2011. Cosmic-ray energy spectrum around the knee observed with the Tibet airshower experiment. *ASTRA* 7, 15–20.
- Battaner, E., Castellano, J., Masip, M., Feb. 2015. Magnetic Fields and Cosmic-Ray Anisotropies at TeV Energies. *Astrophys. J.* 799, 157.
- BenZvi, S., Jul. 2014. Observations of the anisotropy of cosmic rays at TeV-PeV. *ASTRA Proceedings* 1, 33–37.
- Biermann, P. L., Caramete, L. I., Meli, A., Nath, B. N., Seo, E.-S., de Souza, V., Becker Tjus, J., Oct. 2015. Cosmic ray transport and anisotropies to high energies. *ASTRA Proceedings* 2, 39–44.
- Desiati, P., Apr. 2014. Observation of TeV-PeV cosmic ray anisotropy with IceCube, IceTop and AMANDA. *Nuclear Instruments and Methods in Physics Research A* 742, 199–202.
- Desiati, P., Lazarian, A., Oct. 2014. TeV Cosmic Ray Anisotropy and the Heliospheric Magnetic Field. *ASTRA Proceedings* 1, 65–71.
- Di Sciascio, G., Sep. 2015. The cosmic ray anisotropy below  $10^{15}$  eV. *ASTRA Proceedings* 2, 27–33.
- Di Sciascio, G., Iuppa, R., Jul. 2014. On the Observation of the Cosmic Ray Anisotropy below  $10^{15}$  eV. ArXiv e-prints.
- Effenberger, F., Fichtner, H., Scherer, K., Büsching, I., Nov. 2012. Anisotropic diffusion of Galactic cosmic ray protons and their steady-state azimuthal distribution. *Astron. & Astrophys.* 547, A120.
- Giacinti, G., Sigl, G., Aug. 2012. Local Magnetic Turbulence and TeV-PeV Cosmic Ray Anisotropies. *Physical Review Letters* 109 (7), 071101.
- Glushkov, A. V., Pravdin, M. I., Feb. 2013. Variable anisotropy of cosmic rays with  $E_0 < 10^{18}$  eV from Yakutsk EAS array data. *Astronomy Letters* 39, 65–71.
- Harari, D., Mollerach, S., Roulet, E., Mar. 2016. Angular distribution of cosmic rays from an individual source in a turbulent magnetic field. *Phys. Rev. D* 93 (6), 063002.
- Haverkorn, M., Spangler, S. R., Oct. 2013. Plasma Diagnostics of the Interstellar Medium with Radio Astronomy. *Space Sci. Rev.* 178, 483–511.
- IceCube Collaboration, Aartsen, M. G., Abraham, K., Ackermann, M., Adams, J., Aguilar, J. A., Ahlers, M., Ahrens, M., Altmann, D., Anderson, T., et al., Mar. 2016. Anisotropy in Cosmic-Ray Arrival Directions in the Southern Hemisphere with Six Years of Data from the IceCube Detector. ArXiv e-prints.
- Iuppa, R., ARGO-YBJ Collaboration, Feb. 2013. Multi-scale TeV cosmic-ray anisotropy observed with the ARGO-YBJ experiment. *Journal of Physics Conference Series* 409 (1), 012039.
- Iuppa, R., Di Sciascio, G., ARGO-YBJ Collaboration, Nov. 2012. Cosmic-ray anisotropies observed by the ARGO-YBJ experiment. *Nuclear Instruments and Methods in Physics Research A* 692, 160–164.
- Kopp, A., Büsching, I., Strauss, R. D., Potgieter, M. S., Mar. 2012. A stochastic differential equation code for multidimensional Fokker-Planck type problems. *Computer Physics Communications* 183, 530–542.
- Kóta, J., Jokipii, J. R., Feb. 2014. Are Cosmic Rays Modulated beyond the Heliopause? *Astrophys. J.* 782, 24.
- Kumar, R., Eichler, D., Apr. 2014. Large-scale Anisotropy of TeV-band Cosmic Rays. *Astrophys. J.* 785, 129.
- Linsky, J. L., Redfield, S., Nov. 2014. The local ISM in three dimensions: kinematics, morphology and physical properties. *Astrophys. Space Sci.* 354, 29–34.
- López-Barquero, V., Farber, R., Xu, S., Desiati, P., Lazarian, A., Sep. 2015. Cosmic Ray Small Scale Anisotropies

- and Local Turbulent Magnetic Fields. ArXiv e-prints.
- Luo, X., Zhang, M., Potgieter, M., Feng, X., Pogorelov, N. V., Jul. 2015. A Numerical Simulation of Cosmic-Ray Modulation Near the Heliopause. *Astrophys. J.* 808, 82.
- Mackey, J., Gvaramadze, V. V., Mohamed, S., Langer, N., Jan. 2015. Wind bubbles within H ii regions around slowly moving stars. *Astron. & Astrophys.* 573, A10.
- Mertsch, P., Funk, S., Jan. 2015. Solution to the Cosmic Ray Anisotropy Problem. *Physical Review Letters* 114 (2), 021101.
- Parker, E. N., 1965. The passage of energetic charged particles through interplanetary space. *Planet. Space Sci.* 13, 9–49.
- Pierre Auger Collaboration, Abreu, P., Aglietta, M., Ahlers, M., Ahn, E. J., Albuquerque, I. F. M., Allard, D., Allekotte, I., Allen, J., Allison, P., et al., Jan. 2013. Constraints on the Origin of Cosmic Rays above  $10^{18}$  eV from Large-scale Anisotropy Searches in Data of the Pierre Auger Observatory. *Astrophys. J. Lett.* 762, L13.
- Pierre Auger Collaboration, Abreu, P., Aglietta, M., Ahn, E. J., Albuquerque, I. F. M., Allard, D., Allekotte, I., Allen, J., Allison, P., Alvarez Castillo, J., et al., Mar. 2011. Search for first harmonic modulation in the right ascension distribution of cosmic rays detected at the Pierre Auger Observatory. *Astroparticle Physics* 34, 627–639.
- Pogorelov, N. V., Borovikov, S. N., Heerikhuisen, J., Zhang, M., Oct. 2015. The Heliotail. *Astrophys. J. Lett.* 812, L6.
- Potgieter, M., Oct. 2014. Very Local Interstellar Spectra for Galactic Electrons, Protons and Helium. *Brazilian Journal of Physics* 44, 581–588.
- Scherer, K., Fichtner, H., Kleimann, J., Wiengarten, T., Bomans, D. J., Weis, K., Feb. 2016. Shock structures of astrospheres. *Astron. & Astrophys.* 586, A111.
- Scherer, K., Fichtner, H., Strauss, R. D., Ferreira, S. E. S., Potgieter, M. S., Fahr, H.-J., Jul. 2011. On Cosmic Ray Modulation beyond the Heliopause: Where is the Modulation Boundary? *Astrophys. J.* 735, 128–+.
- Scherer, K., van der Schyff, A., Bomans, D. J., Ferreira, S. E. S., Fichtner, H., Kleimann, J., Strauss, R. D., Weis, K., Wiengarten, T., Wodzinski, T., Apr. 2015. Cosmic rays in astrospheres. *Astron. & Astrophys.* 576, A97.
- Schwadron, N. A., Adams, F. C., Christian, E., Desiati, P., Frisch, P., Funsten, H. O., Jokipii, J. R., McComas, D. J., Moebius, E., Zank, G. P., Jan. 2015. Anisotropies in TeV Cosmic Rays Related to the Local Interstellar Magnetic Field from the IBEX Ribbon. *Journal of Physics Conference Series* 577 (1), 012023.
- Stanimirović, S., Weisberg, J. M., Pei, Z., Tuttle, K., Green, J. T., Sep. 2010. Arecibo Multi-epoch H I Absorption Measurements Against Pulsars: Tiny-scale Atomic Structure. *Astrophys. J.* 720, 415–434.
- Strauss, R. D., Potgieter, M. S., Büsching, I., Kopp, A., Jul. 2011a. Modeling the Modulation of Galactic and Jovian Electrons by Stochastic Processes. *Astrophys. J.* 735, 83.
- Strauss, R. D., Potgieter, M. S., Ferreira, S. E. S., Fichtner, H., Scherer, K., Mar. 2013. Cosmic Ray Modulation Beyond the Heliopause: A Hybrid Modeling Approach. *Astrophys. J. Lett.* 765, L18.
- Strauss, R. D., Potgieter, M. S., Kopp, A., Büsching, I., Dec. 2011b. On the propagation times and energy losses of cosmic rays in the heliosphere. *J. Geophys. Res.* 116, 12105.
- Toalá, J. A., Arthur, S. J., Aug. 2011. Radiation-hydrodynamic Models of the Evolving Circumstellar Medium around Massive Stars. *Astrophys. J.* 737, 100.
- Toscano, S., IceCube Collaboration, Nov. 2012. Observation of anisotropy in the arrival direction distribution of cosmic rays above TeV energies with IceCube. *Nuclear Instruments and Methods in Physics Research A* 692, 165–169.
- Zhang, M., Zuo, P., Pogorelov, N., Jul. 2014. Heliospheric Influence on the Anisotropy of TeV Cosmic Rays. *Astrophys. J.* 790, 5.
- Zotov, M. Y., Kulikov, G. V., Nov. 2012. A search for small-scale anisotropy of PeV cosmic rays. *Astronomy Letters* 38, 731–743.